

Finite-Difference Relaxation for Parallel Computation of Ionized Field of HVDC Lines

Peng Liu , *Student Member, IEEE*, and Venkata Dinavahi, *Senior Member, IEEE*

Abstract—Ionized field calculations for high-voltage direct current (HVDC) transmission line is a computationally demanding problem, which can benefit from the application of massively parallel high-performance compute architectures. The finite element method (FEM) commonly employed to solve this problem is both memory and execution time intensive. In this paper, a finite-difference relaxation (FDR) method is proposed to solve a unipolar and a bipolar ionized field problem in an HVDC line. The novel FDR method has several advantages over FEM. First, the scheme is suitable for massively parallel computation and runs much faster: Compared with the commercial FEM software Comsol Multiphysics, the speed-up is more than 14 times in CPU parallelization and 35 times in graphics processor parallel implementation, while providing high accuracy. Moreover, the set of equations in FDR need not be assembled; instead, it is solved by a relaxation scheme and requires much less memory than FEM. Additionally, differentiated grid size with interpolation techniques is proposed to improve the flexibility of FDR for problem domain containing irregular geometries or disproportional sizes.

Index Terms—Finite-difference method, graphics processors, HVDC lines, ionized field, Jacobi method, multi-core, many-core, parallel algorithms, relaxation.

I. INTRODUCTION

HIGH-VOLTAGE direct current has such advantages as lower cost and lower power loss over alternating current for bulk power transmission over long distance that new projects are spouting up world-wide. Environmental problems caused by the occurrence of corona on the high voltage conductor have received much attention with the widespread use of HVDC transmission lines in the last few decades.

Since these transmission lines are generally operated above their corona onset voltage, space charges are generated around the energized conductor. These space charges migrate in a manner determined by the electric field; at the same time, the electric field is modified by these space charges. The mutual interaction of electric field and space charges eventually leads to an sustained steady-state, which is governed by Poisson's equation

Manuscript received September 20, 2016; revised December 14, 2016 and January 16, 2017; accepted January 26, 2017. Date of publication January 31, 2017; date of current version January 22, 2018. This work was supported by the Natural Science and Engineering Research Council of Canada. The work of P. Liu was supported by China Scholarship Council (CSC) under Grant 201506120058. Paper no. TPWRD-01132-2016.

The authors are with the Department of Electrical and Computer Engineering, University of Alberta, Edmonton, AB T6G 2R3, Canada (e-mail: pliu3@ualberta.ca; dinavahi@ualberta.ca).

Color versions of one or more of the figures in this paper are available online at <http://ieeexplore.ieee.org>.

Digital Object Identifier 10.1109/TPWRD.2017.2661845

and current continuity equation for unipolar lines [1]. The physical details of the corona and the mutual interaction process are often deemphasized, therefore investigators usually focused on obtaining the solution of the mathematical model, which can be necessarily described by coupled nonlinear partial differential equations (PDE) for 2-D problems.

The analytical solution of an ionized field was first obtained by Townsend in 1914 although it was only applicable for cases with regular geometry such as concentric spheres or coaxial cylinders [2]. For such 2-D problems as conductor-to-ground arrangements, the solutions of the coupled nonlinear PDEs relied on some simplifying assumptions, among which Deutsch's assumption was exclusively employed by investigators before the 1970s [1]. Deutsch's assumption reduced the 2-D problem to 1-D computation along flux lines by assuming that the space charges affect only the magnitude and not the direction of the electric field [3]. This assumption is still utilized in methods such as the flux tracing method owing to its simplicity [4]–[6]. Janischewskij *et al.* for the first time solved the PDEs without resorting to Deutsch's assumption using the finite element method in 1979 [7]. Then Takuma *et al.* in 1981 proposed the upstream FEM to overcome numerical instability caused by the accumulated error in each iteration [8]. To handle the nonlinearity of the problem, both [7] and [8] solved the coupled equations iteratively based on a predictor-corrector algorithm. Thereafter FEM was dominantly used in ionized field calculation. More complicated configurations which considered the effect of wind velocity, bipolar conductors and bundled conductors were investigated using FEM in [9]–[15]. Improved Galerkin method based FEM, combination of FEM with the method of characteristics or the finite volume method, and other numerical techniques and iterative strategies were proposed to make the calculation more stable and more efficient in [16]–[21]. Recently 3-D FEM was also explored to solve the ionized field in the presence of human bodies and buildings in [22]–[25].

Nevertheless, it's generally highly acknowledged that FEM is CPU and memory intensive, particularly for those cases where a large number of discretized nodes and repeat calculations are necessary. Nowadays high-performance parallel computing is being explored to speed up iterative linear solvers, among which the conjugate gradient (CG) solver is most widely employed. Based on [26], the Jacobi method has advantages over CG method when applied in MapReduce framework, which is based on a single instruction stream multiple data stream (SIMD) paradigm. However, the prerequisite of Jacobi method that the system of linear equations should be diagonally

dominant restricted its use in a FEM solver. In addition, graphics processors (GPUs) as another commonly used SIMD paradigm are limited by the device memory for large-scale FEM problems [27]. GPUs have been exploited for the simulation of large-scale power systems in several areas including transient stability simulation, electromagnetic transient simulation, and dynamic state estimation [28]–[31].

In this paper, a novel finite difference relaxation (FDR) method is proposed to solve a unipolar and a bipolar conductor-to-ground problem without Deutsch's assumption. This method requires much less memory than FEM because the finite-difference equations need not be assembled. And FDR can be massively parallelized in the GPU. The parallel implementations are carried out on multi-core CPU and many-core GPU, and the results are compared with those obtained from commercial FEM software Comsol Multiphysics with regard to accuracy and computational efficiency. Additionally, for the bipolar case, the current continuity equations are regarded as PDEs on electric potential rather than on ion density, and the solution process using the FDR scheme is unconditionally stable.

This paper is organized as follows. Section II presents the assumptions, the governing equations, the boundary conditions, and the iterative scheme. Section III provides the implementation details of the FDR method with differentiated grid size. Section IV gives the unipolar and bipolar case studies and the result comparison of the FDR method and the FEM. Finally, Section V presents the conclusion.

II. PROBLEM DESCRIPTION

A. Assumptions for Modeling

Since corona and the ionized field are complicated physical phenomena, appropriate assumptions are necessary to build a solvable mathematical model. The assumptions employed in this paper are the following:

- 1) The ionized field is time-independent. All parameters involved do not vary along the direction of the transmission line, i.e. the problem is two-dimensional.
- 2) The thickness of the ionization layer around the conductor is so small as to be neglected.
- 3) Ionic mobility is constant, and ion diffusion is neglected.
- 4) The electric potential of those nodes on the artificial boundary is determined by the space charge free field, which is defined by Laplacian equations.

The 2-D ionized field problem is a boundary value problem (BVP), and the problem domain can be illustrated as in Fig. 1. The rectangular domain may contain bipolar bundled conductors or a single centered conductor for different cases.

B. Governing Equations

The governing equations of the bipolar ionized field are

$$\nabla^2 \cdot \varphi = \frac{\rho^- - \rho^+}{\epsilon_0}, \quad (1)$$

$$\nabla \cdot (k^+ \rho^+ \nabla \varphi) = \frac{R \rho^+ \rho^-}{e}, \quad (2)$$

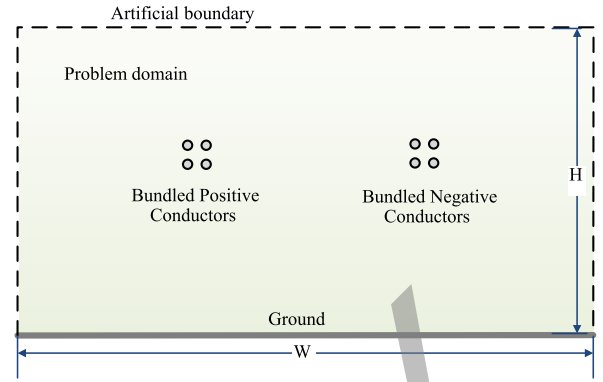


Fig. 1. Computational domain for bipolar conductor-to-ground arrangement.

$$\nabla \cdot (k^- \rho^- \nabla \varphi) = \frac{R \rho^+ \rho^-}{e}, \quad (3)$$

where ρ is the space charge density, ϵ_0 the permittivity of free space, φ the electric potential, k the ionic mobility, R is the recombination rate, e the charge of the electron, and the superscript + for positive and - for negative.

The three unknowns to be solved in the bipolar ionized field problem are electric potential φ and the space charge densities ρ^+ and ρ^- .

In the case of unipolar ionized fields, all the space charges have the same polarity as the conductor. The governing equations of the unipolar ionized field with only positive conductor can be obtained by forcing the negative space charge density to 0. The unknowns to be solved are electric potential φ and the positive space charge density ρ^+ . Equations (1)–(3) are reduced to the following:

$$\nabla^2 \cdot \varphi = -\frac{\rho^+}{\epsilon_0}, \quad (4)$$

$$\nabla \cdot (\rho^+ \nabla \varphi) = 0. \quad (5)$$

C. Boundary Conditions

The product of two unknowns in the current continuity equation makes the problem nonlinear. The solution of the BVP can be solved if the boundary conditions (BCs) are well-posed, i.e., neither undetermined nor overdetermined. Substituting (4) to (5) yields the following equation:

$$\nabla \cdot ((-\epsilon_0 \nabla^2 \cdot \varphi) \nabla \varphi) = 0. \quad (6)$$

(6) is a nonlinear third-order PDE on φ , and three boundary conditions on φ are required:

- 1) The electric potential on the conductor is the applied voltage V_0 (Dirichlet type):

$$\varphi_C = V_0. \quad (7)$$

- 2) The ground is taken as the reference (Dirichlet type):

$$\varphi_G = 0. \quad (8)$$

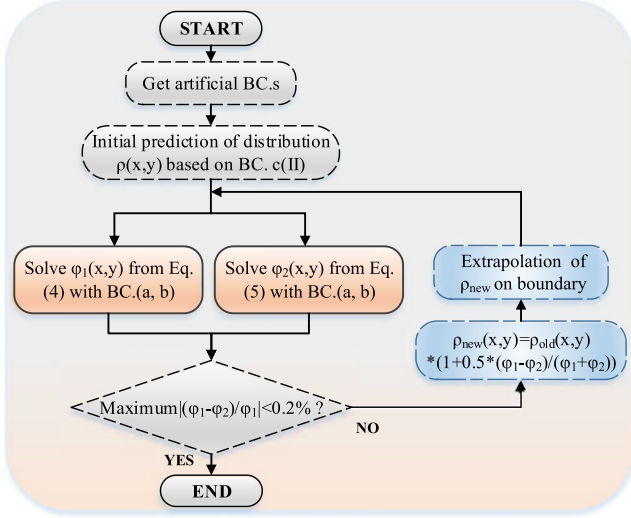


Fig. 2. Flow chart of the predictor-corrector algorithm.

- 3) The third boundary condition is usually selected from the following two conditions. Only one can be applied or the problem will be overdetermined.
- The electric field strength at the conductor surface is constant at the corona onset value (Kaptzov's assumption, Neumann type):

$$\frac{\partial \varphi}{\partial n} = E_0. \quad (9)$$

- The charge density at the conductor surface is known as ρ_0 from experimental results:

$$\rho_C = \rho_0. \quad (10)$$

In addition, truncation of the domain is necessary. The above boundary conditions together with the previous assumption (4) can define the problem well.

D. Predictor-Corrector Strategy

For the unipolar case, the problem could not be resolved directly because the governing PDEs containing the two unknowns are coupled. The predictor-corrector algorithm proposed by [7] and [8] is based on the fact that both (4) and (5) can be solved once one unknown is assigned an initially predicted distribution. Then the predicted distribution is corrected progressively by iteratively solving the two PDEs. One most common and simple iterative procedures in [7] can be described as in Fig. 2. The iterative strategy used may be a bit different yet the same solution can be achieved. For example, in [8], $\varphi_1(x, y)$ solved from (4) was sequentially utilized by (5) to generate a new $\rho(x, y)$. In this paper, the flow chart shown in Fig. 2 is employed for the unipolar case.

For the bipolar case, the iterative strategy to handle φ , ρ^+ and ρ^- is very similar. The modified iterative strategy for the three unknowns is presented in Section V.

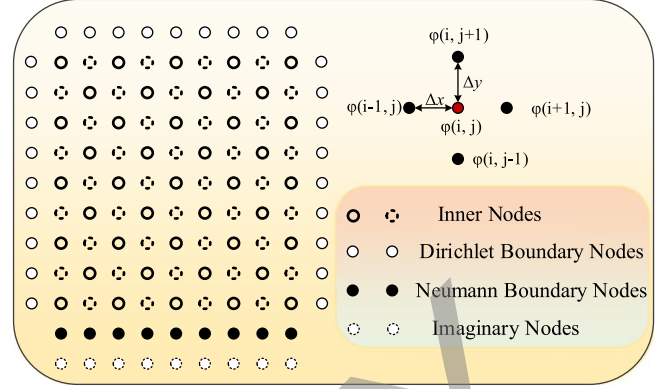


Fig. 3. Domain discretization for 2-D boundary value problem.

III. FINITE-DIFFERENCE RELAXATION METHODOLOGY

A. Domain Discretization and FDR

The weighted residual method in FEM is widely utilized instead of tediously constructing a functional based on the variational principle. The product of residual and weighted function is integrated over the domain of each element, and a set of equations associated with nodes of each element can be obtained by forcing the integration to be zero. Then these equations are assembled and solved based on certain boundary conditions.

On the contrary, the finite-difference method is convenient when forming equations by replacing derivative with difference quotient in classic formulation; at the same time, a regular grid is required. Fig. 3 shows a simple 2-D discretized domain. The order of the PDE determines the number of nodes required for difference equation derivation. For a second order PDE, the five-nodes mode is sufficient. As shown in Fig. 3, every inner node is surrounded by four nodes (either inner or boundary nodes). A very important observation in [7] is that both the Poisson's equation and the current continuity equation can be rewritten as the following second-order PDE on φ :

$$\nabla \cdot (\alpha \nabla \varphi) = \beta. \quad (11)$$

Equations (1)–(5) can be obtained by setting different α and β . For example, (1) in 2-D domain can be rewritten as the following form when $\alpha = 1$ and $\beta = (\rho^- - \rho^+) / \epsilon_0$:

$$\frac{\partial^2 \varphi}{\partial x^2} + \frac{\partial^2 \varphi}{\partial y^2} = \frac{\rho^- - \rho^+}{\epsilon_0}. \quad (12)$$

The second derivative in (12) can be replaced with a difference equation at node (i, j) using central difference scheme in the five-nodes mode as:

$$\frac{\partial^2 \varphi}{\partial x^2} = \frac{\varphi(i-1, j) + \varphi(i+1, j) - 2\varphi(i, j)}{\Delta^2 x}, \quad (13)$$

$$\frac{\partial^2 \varphi}{\partial y^2} = \frac{\varphi(i, j-1) + \varphi(i, j+1) - 2\varphi(i, j)}{\Delta^2 y}. \quad (14)$$

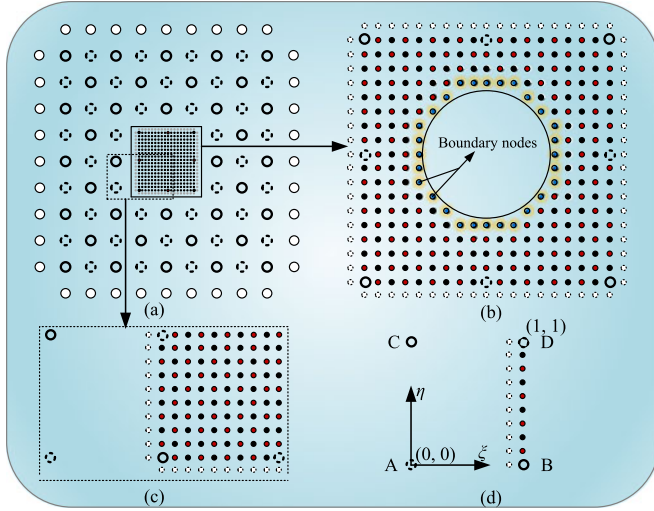


Fig. 4. Differentiated grid size and interpolation in FDR.

Thus Poisson's (1) at node (i, j) can be written as:

$$\varphi(i, j) = \frac{\Delta^2 x \Delta^2 y}{2(\Delta^2 x + \Delta^2 y)} \cdot \left(\frac{\varphi(i-1, j) + \varphi(i+1, j)}{\Delta^2 x} + \frac{\varphi(i, j-1) + \varphi(i, j+1)}{\Delta^2 y} + \frac{\rho^+(i, j) - \rho^-(i, j)}{\epsilon_0} \right). \quad (15)$$

Similarly, setting $\alpha = \rho^+$ and $\beta = 0$, the current continuity equation (5) can be rewritten as:

$$\varphi(i, j) = \frac{\Delta^2 x \Delta^2 y}{2(\Delta^2 x + \Delta^2 y)} \cdot \left(\frac{\varphi(i-1, j) + \varphi(i+1, j)}{\Delta^2 x} + \frac{\varphi(i, j-1) + \varphi(i, j+1)}{\Delta^2 y} + \frac{\rho(i, j)}{\epsilon_0} + \frac{(\rho^+(i+1, j) - \rho^+(i-1, j))(\varphi(i+1, j) - \varphi(i-1, j))}{4\Delta^2 x} + \frac{(\rho^+(i, j+1) - \rho^+(i, j-1))(\varphi(i, j+1) - \varphi(i, j-1))}{4\Delta^2 y} \right). \quad (16)$$

For those nodes on the boundary, the BCs can be either Dirichlet type or Neumann type. Nodes located exactly on regular boundary (such as a line) are straightforward while nodes near the circular conductor need special attention. For example, in this paper, those nodes satisfying the following conditions define the approximated conductor surface (Fig. 4(b)):

$$r < d < r + \sqrt{\Delta^2 x + \Delta^2 y} \quad (17)$$

where d is the distance between a node and the conductor center, r the conductor radius, and Δx , Δy are the spatial increment. The approximation is more accurate when the grid layer is finer. The values of the nodes on Dirichlet boundary are fixed and only used as known value when updating the adjacent inner nodes. Thus the finite difference equation applies only for inner nodes and no equations are necessary for boundary nodes. For nodes on

Neumann boundary, the equation can be written with the help of imaginary nodes, which are associated with inner nodes and $\frac{\partial \varphi}{\partial n}$.

By writing the difference equation for each node, a set of linear equations can also be obtained as in FEM. In FEM assembling all the element equations often produces a large matrix which calls for more memory, although the sparsity of the matrix may enable saving of memory by exploring special data storage methods. Undoubtedly, the tedious tasks undermine the prospect for massively parallel computation. The solution phase of FDR is quite different.

Indeed calculating one node based on the adjacent 4 nodes by (15) can be regarded as a form of communication or information exchange. At first glance, a single communication between one node and its neighbors is probably meaningless because it never knows whether the neighbors are of the desired solutions or not. However, if all inner nodes update themselves repeatedly, these communications can be very beneficial to find the final solution. Intuitively, the prescribed value such as information on the boundary will gradually flow into the entire domain by iteratively updating each node. Convergence can be expected when all values of inner nodes satisfy (15) if the problem is well-posed. Each node is concerned with its own computation based on the finite-difference equations and eventually a converged solution satisfying all nodes can be achieved. Thus, the process is called *finite-difference relaxation*. The following section will reveal that the convergence of the FDR scheme is a mathematical certainty.

B. Jacobi Method and Convergence Condition

There are two classes of algorithms for solving a linear system of equations. Direct methods like Gauss elimination, or equivalently LU factorization followed by back-substitution can provide the exact solution after a finite sequence of operations. Iterative methods such as the conjugate gradient method and the Jacobi method are commonly used as they provide solutions for desired error tolerances for a large-scale linear system. Indeed, for Poisson's equation, the set of finite-difference equations can be written as the general form:

$$\mathbf{A}\mathbf{x} = \mathbf{b}, \quad (18)$$

where \mathbf{A} is a known sparse matrix associated with the coefficients of each unknown nodes and its neighbors indicated in (15), \mathbf{x} the unknown vector containing $\varphi(i, j)$ of each unknown node (boundary node excluded) and \mathbf{b} the known vector related to $(\rho^-(i, j) - \rho^+(i, j))/\epsilon_0$ and prescribed boundary values.

Note that most unknown nodes are surrounded by four other unknown nodes, and the nodes right adjacent to the boundary nodes have only two or three unknown neighbors.

Solution of the system can be obtained by the iterative expression:

$$\mathbf{P}\mathbf{x}^{k+1} = (\mathbf{P} - \mathbf{A})\mathbf{x}^k + \mathbf{b}, \quad (19)$$

where \mathbf{P} is the preconditioner and \mathbf{x}^k is the k^{th} approximation of \mathbf{x} .

For the Jacobi method, the preconditioner \mathbf{P} is set the diagonal matrix of \mathbf{A} . Indeed, \mathbf{A} can be decomposed into a diagonal

matrix D , and the remainder R . Thus the iteration formula for Jacobi method can be written as:

$$\mathbf{x}^{k+1} = -D^{-1}R\mathbf{x}^k + D^{-1}\mathbf{b}. \quad (20)$$

The standard convergence condition is when the spectral radius of the iteration matrix is less than 1 [32], namely

$$\rho(D^{-1}R) < 1. \quad (21)$$

It is acknowledged that (21) is sufficiently satisfied if the matrix is diagonally dominant, i.e., the absolute value of the diagonal term is greater than the sum of absolute values of other terms:

$$|a_{ii}| > \sum_{j \neq i} |a_{ij}|. \quad (22)$$

It can be observed from (15) that the coefficient of each to-be-updated inner node is equal to the summation of coefficients of its four unknown neighbors, and the coefficient of those to-be-updated nodes right adjacent to the boundary nodes is greater than the summation of coefficients of its two or three unknown neighbors. Thus, for most rows in coefficient matrix A , the following equation is satisfied:

$$|a_{ii}| = \sum_{j \neq i} |a_{ij}|. \quad (23)$$

If (23) is satisfied for all rows of A , the spectral radius is equal to 1. However, for those nodes next to the known boundary nodes, (22) is well satisfied for the corresponding row of A and determine that the spectral radius is less than 1.

C. Differentiated Grid Size

Few attempts using finite-difference method have been reported in the literature due to the inflexibility when handling irregular geometries and disproportional sizes. For example, in the ionized field problem handled by FEM, the mesh size near the conductor is fine enough to ensure accuracy while a relatively coarse mesh is applied for the rest of the vast domain to save computational resources. A square grid is the basis of FDR, and it is one drawback compared with FEM. In order to depict the contour of the thin conductor, high node density (or fine grid) is needed around the conductor. And if the whole domain is filled with these dense nodes, the merits of FDR will be impaired seriously. Whereas differentiated grid sizes can be explored and the details are described below.

Fig. 4(a) shows a simplified scheme for applying two layers with differentiated grid sizes. Fig. 4(b) shows irregular geometries can be described accurately if the grid is fine enough. Undoubtedly different mesh sizes will cause the communication problem on the boundary separating the two layers. As shown in Fig. 4(c), updating the outermost nodes of the fine grid will require the value of some non-existing nodes next to them, which are the dashed nodes located out of the fine grid layer. However, even though these dashed nodes are imaginary, their values can be predicted as they are located in a cell (a square consisting of four adjacent nodes) in the coarse grid. Therefore, an interpolation technique similar with that of FEM is employed to predict

the desired value based on the nodes in the coarse grid layer. Fig. 4(d) shows a local coordinate system. Assume the electric potential at nodes A , B , C and D are φ_A , φ_B , φ_C and φ_D . For any coordinate (ξ, η) , the contribution (shape function) of each node N_A , N_B , N_C and N_D can be written as:

$$\begin{cases} N_A = (\xi - 1)(\eta - 1), \\ N_B = \xi(1 - \eta), \\ N_C = \eta(1 - \xi), \\ N_D = \xi\eta. \end{cases} \quad (24)$$

Thus the interpolated value at any coordinate (ξ, η) can be predicted as:

$$\varphi(\xi, \eta) = N_A\varphi_A + N_B\varphi_B + N_C\varphi_C + N_D\varphi_D. \quad (25)$$

By interpolation, the fine grid layer can obtain information from the coarse grid layer. It should be noted that after all nodes are updated, a similar process called retrieval is necessary so that the coarse grid layer can obtain information from the fine grid layer. The detailed process and the according node type are described in the flow chart in Fig. 5. Thus, for each iteration, the following three phases are always necessary for differentiated grid sizes:

- 1) Interpolation: information flows from the coarse grid layer to the fine grid layer.
- 2) Updating: each node is updated based on its neighbors.
- 3) Retrieval: information flows from the fine grid layer back to the coarse grid layer.

IV. MASSIVELY PARALLEL IMPLEMENTATION

A. Data Dependency and Parallelism

As discussed above, once \mathbf{x}^k is available, \mathbf{x}^{k+1} can be obtained. Though nodes can be calculated independently, synchronization is necessary between iterations to avoid updating one node with its yet-to-be-updated neighbors multiple times. Additionally, the interpolation and retrieval phase can also be parallelized in each iteration, yet synchronization is also needed between these phases.

In the FDR process, two matrices are needed for each variable to store the node values of both coarse grid layer and fine grid layer. To elaborate the process flowchart clearly, different node types are classified based on the location (shown in Fig. 5(a)). For example, type A, a, B and b are the solid and dashed inner nodes in the two layers. Type C and c are boundary nodes while type D and d represent the nodes to be updated in the retrieval phase. The main flowchart is shown in Fig. 5(c).

B. Parallelization on CPU and GPU

The FDR program is parallelized on both multi-core CPU and many-core GPU.

For CPU parallelization, multiple threads are launched by the master thread and handle different parts of the tasks. Open multi-processing (OpenMP) and POSIX Threads (Pthread) are commonly used application programming interfaces (API) for shared memory multiprocessor programming. OpenMP is relatively higher level, and thus easier to use. The high-level

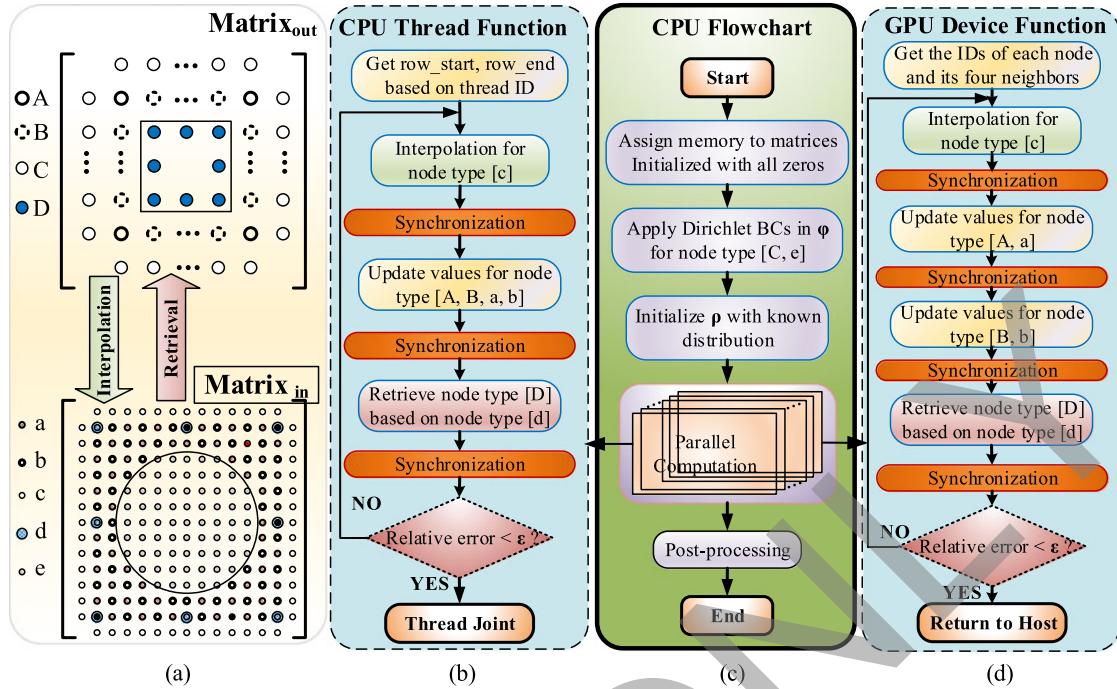


Fig. 5. Massively parallel implementation of FDR scheme on CPU and GPU.

feature results in inflexibility because it is difficult to control each thread. Moreover, for the FDR iterative scheme, repeatedly launching and joining threads between iterations greatly increases overhead for OpenMP. On the contrary, Pthread is a lower level API that takes extremely fine-grained control over threads. Each thread is launched and will not be joined until the iteration process ends. Therefore, Pthread is utilized to implement the CPU parallelization in this work. Considering the number of cores available in CPU, the row-wise parallel implementation is employed, and the flowchart of the thread function is described in Fig. 5(b).

Indeed, massive parallelization is perfectly suitable for the updating phase because node calculations do not depend on each other. CUDA is chosen for massive-thread parallel programming on the GPU. A CUDA program separates the hardware resources into CPU side (host) and GPU side (device). There is no shared memory for two sides and thus copy operations are necessary for data exchange.

In the CPU parallelization, each variable needs a copy operation to store the updated value. A more efficient strategy is explored for GPU implementation to reduce the required memory and accelerate the convergence. Indeed, it can be observed that for all inner nodes in Fig. 4, all solid nodes are surrounded by four dashed nodes and vice versa. Thus the calculation phase can be separated into two steps: calculating all solid nodes in parallel, and sequentially updating all the dashed nodes in parallel. In other words, the updated values of the solid nodes are utilized by updating the dashed nodes within one iteration. It is applicable for both the coarse grid layer and the fine grid layer. This scheme is similar to the Gauss-Seidel method, and the convergence is faster than that of the Jacobi method. The flowchart of the device function is shown in Fig. 5(d).

The detailed parameters of the CPU and GPU are described in Appendix A.

V. CASE STUDY AND RESULTS COMPARISON

A. Unipolar Case Study

1) *Result Comparison of FDR vs FEM*: Both Poisson's (4) and current continuity (5) can be solved with FDR if the distribution of space charge is provided. On the other hand, the problem can also be solved with the equation-based modeling in Comsol Multiphysics. Poisson's equation is chosen in the case study to comprehensively compare the FDR method and the FEM. The parameters are shown in the Appendix B.

In order to obtain reliable results from FEM, mesh dependency test is done on a sample point. It turned out that the FEM results can be regarded as stable and reliable when the number of nodes is more than 1500 in the case. Thus the FEM results are assumed correct and can serve as a benchmark for evaluating the accuracy of FDR.

Since the problem domain is 2-D, the sample line shown in Fig. 1 is selected to plot the results clearly. The electric potential along the selected path solved from both FEM and FDR is shown in Fig. 6. When the number of nodes is 10,000, the maximum relative difference between the FEM and the FDR method is around 3%.

It is clear that the results of FDR converge to the results of FEM when the maximum relative error ϵ between iterations decreases. As an iterative method, the solution phase of FDR can be described by the ϵ -iteration curve shown in Fig. 7. The convergence speed is determined by the spectral radius mentioned above; convergence is faster when the spectral radius is small. When the problem size increases, the percentage of

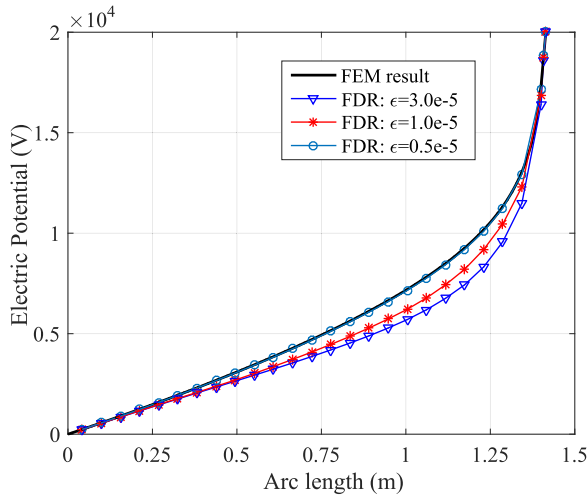


Fig. 6. Electric potential comparison of FEM and FDR for unipolar case.

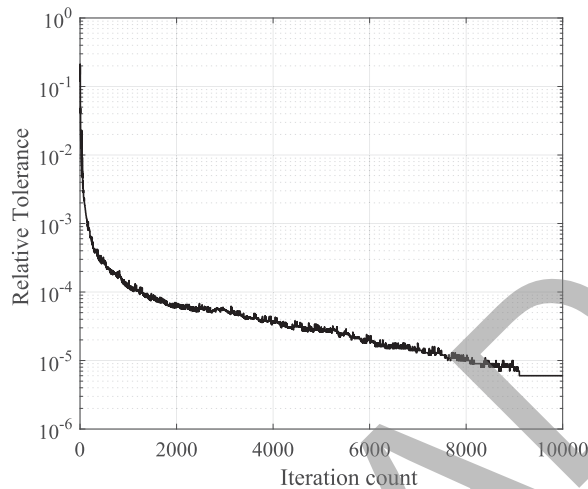


Fig. 7. Relative error vs iteration number for the FDR method.

boundary nodes decreases, and the spectral radius comes closer to 1. However, to the author's knowledge, it is difficult to quantify the relationship of node number, spectral radius, and ϵ . It was found from experience that the iteration can be deemed convergent when ϵ is less than 10^{-6} if the number of nodes is less than 50,000.

2) *Accuracy and Efficiency Comparison of FDR vs FEM:* A comprehensive comparison of FDR and FEM with regard to computation time and accuracy is presented in Table I. For the CPU parallel implementation utilizing 16 processor cores, the maximum speed-up is greater than 14 under different node numbers. For GPU parallel implementation, the speedup is 30 times. As shown in the last column of Table I, the results of FDR come closer to the correct solution as the number of nodes increases.

Note that the built-in direct solver of Comsol Multiphysics is applied, which turned out to be faster than its iterative solver for the cases presented in the table. For example, the iterative solver consumed 7.1 s while the direct solver consumed 5.56 s when the node number is 40,000. Thus the speedup is with

respect to the execution time of the commercial software Comsol Multiphysics, which can be regarded as highly optimized and sufficiently efficient.

Similarly, the current continuity equation was simulated with the proposed FDR scheme. Applying the iterative strategy in Fig. 2, the final solution was obtained. The initial distribution of $\rho(x, y)$ and the solved $\varphi_1(x, y)$ and $\varphi_2(x, y)$ are presented in the first row of Fig. 8. When the iteration converges, the final solution of $\rho(x, y)$, $\varphi_1(x, y)$ and $\varphi_2(x, y)$ is shown in the second row of Fig. 8.

B. Practical Bipolar Case Study

1) *Application of FDR:* In practical HVDC applications, bipolar bundled conductors are usually utilized for power transmission. The case is more complicated, whereas the computation can still benefit from the merits of the FDR scheme. The following section will elaborate how the FDR scheme is applied for the full-scale bipolar bundled conductors. Fig. 9 shows the structure of a typical ± 500 kV HVDC lattice tower of the Eastern Alberta HVDC line built by ATCO Electric Ltd., and the geometric parameters are available online [33].

For the bipolar case, space is filled with ions of both polarities. The ions of both polarities migrate to the ground, at the same time, they migrate to the conductors with the opposite polarity.

In each iteration of the solution phase, the φ in (1) is solved with the guessed or updated ρ^+ and ρ^- ; and then the ρ^+ in (2) and the ρ^- in (3) are solved respectively based on the obtained φ in (1). However, the solution process of the current continuity equations is likely to become unstable because of the accumulated error of first-order derivative. Thus to counter instability, it calls for numerical techniques like the upwind scheme in [8]. The current continuity equation in (2) and (3) can be seen as a first order PDE on ρ (either ρ^+ or ρ^-), and it can also be regarded as a second order PDE on φ . Mathematically, the stability of a first order PDE on u is conditional and depends on the coefficients of u , u_x and u_y . However, the second order PDE on φ in (11) can be solved with the FDR scheme efficiently if the distributions of α and β are given (either guessed value or constant) and the solution of the FDR scheme is unconditionally stable. That is why the numerical stability issue is not a concern in [7] as well as in the unipolar case studied above. Since solving ρ^+ based on known φ is unstable while solving φ based on known ρ^+ is unconditionally stable, the iterative strategy in Fig. 2 is improved to solve the bipolar case to avoid numerical instability.

The improved iteration process can be described with the following steps:

- 1) Initial estimate of space charge ρ^+ and ρ^- are provided based on boundary conditions.
- 2) Solve φ in (1), (2) and (3) respectively with the FDR scheme based on the known ρ^+ and ρ^- . The results are stored as φ , φ^+ and φ^- .
- 3) Update ρ^+ based on $\varphi - \varphi^+$ and ρ^- based on $\varphi - \varphi^-$.
- 4) Go to Step 2 with the updated ρ^+ and ρ^- . The process is repeated until the maximum relative error between φ^+ and φ^- is smaller than the prescribed value ϵ .

TABLE I
EFFICIENCY AND ACCURACY COMPARISON OF PROPOSED FDR METHOD WITH FEM

Node number	FEM solution time (s) Comsol Multiphysics	FDR solution time (s) and speed-up								Relative error
		Multi-core CPU				Speed-up	Many-core GPU			
		Solution time - thread count					Solution time	Speed-up		
1	4	8	16							
3600	0.9	0.182	0.065	0.050	0.050	18	0.028	32.1	4.63%	
10,000	1.78	0.700	0.210	0.140	0.124	14.4	0.05	35.6	3.15%	
40,000	5.56	2.960	0.816	0.512	0.38	14.6	0.18	30.8	1.68%	

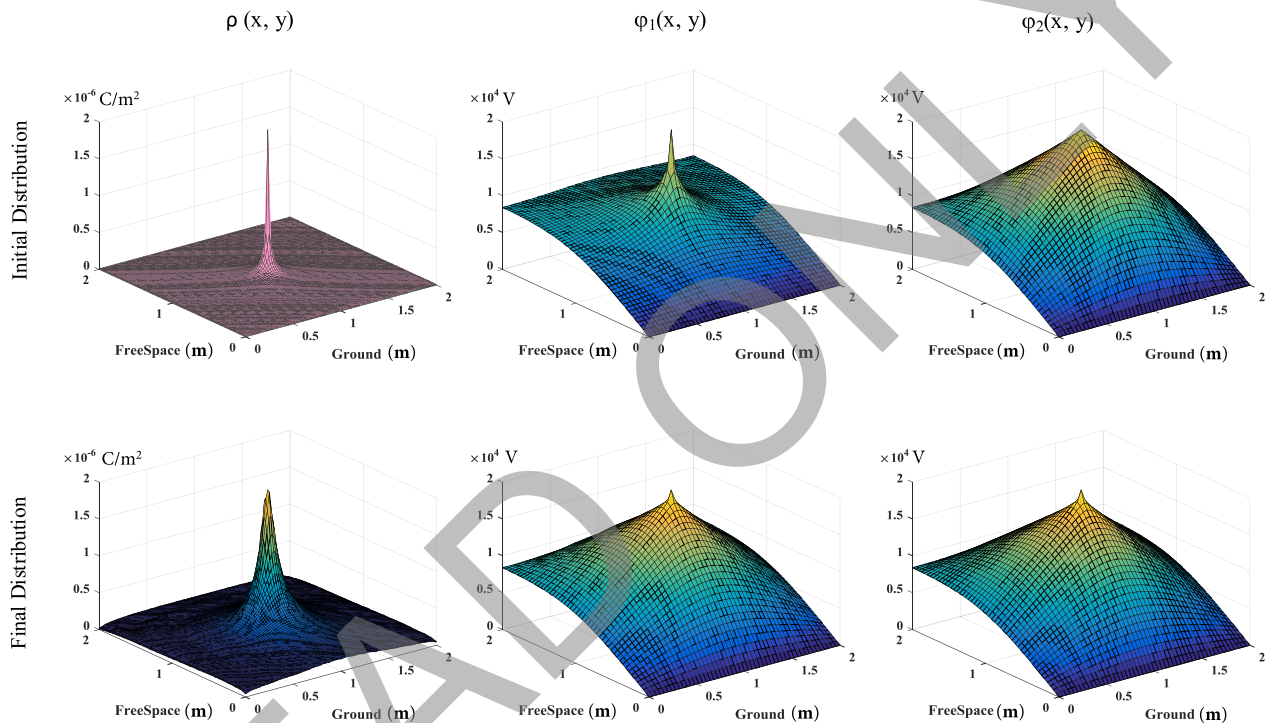


Fig. 8. Final converged solution of the unipolar ionized field attained from the proposed FDR method.

It is worth mentioning that solving (11) with the FDR scheme is basically no different for either the unipolar case or the bipolar case. For the case with multiple conductors, multiple Dirichlet boundary conditions should be applied. Similarly, differentiated grid sizes are employed in consideration of the thin conductor in a vast space domain. As shown in Fig. 10, the fine grid layer is applied around each conductor and the coarse grid layer is applied for the rest domain. The nodes nearest to the conductor in the fine grid layer are defined as Dirichlet boundary nodes and the values are fixed in the FDR scheme. The node updating (communication) pattern stays the same, and both the interpolation and retrieval phase should be applied to every boundary that separates the coarse grid layer and the fine grid layer.

2) *Results and Discussion:* According to the structure shown in Fig. 9, the minimum height of the transmission line is 12 m at the mid-span between towers. Thus the computational domain is obtained by spatial truncation. The width of the truncated problem domain is 80 m and the height 25 m. The

geometric parameters are shown in Fig. 9 and other necessary parameters are presented in Appendix C.

Following the iterative steps listed above, the bipolar problem with bundled conductors can be resolved with both the FEM and the FDR scheme. It turned out the FDR scheme can be perfectly applied in problems with multiple Dirichlet boundary conditions. The result comparison of the calculated electric potential along the sample line using FDR and FEM is shown in Fig. 11. The electric field strength near the ground is shown in Fig. 12 and the contour agrees well with that in [22].

The calculated distribution of the electric potential is shown in the Fig. 13.

The distribution of the positive and negative ion density distribution are presented in the Fig. 14. The results agree with the physical facts that ions of both polarities migrate to the ground and to the conductor with the opposite polarity.

The speed-up of the bipolar case is similar to the unipolar case and can be inferred from Table I. For both cases, repeatedly

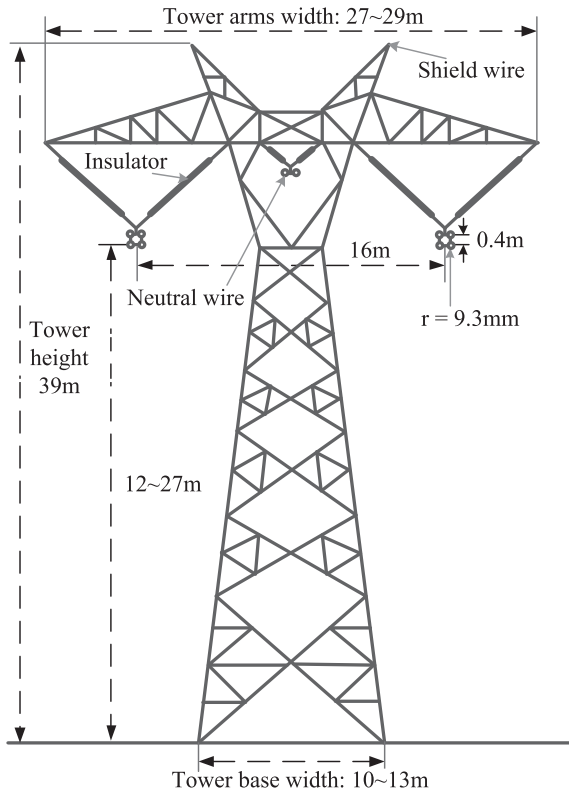


Fig. 9. Structure of ± 500 kV DC lattice tower of the Eastern Alberta HVDC Line.

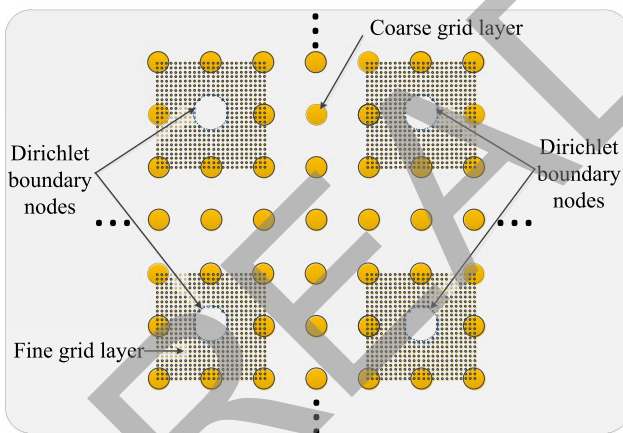


Fig. 10. Differentiated grid layer for multiple Dirichlet boundaries of the 4-conductor bundle.

solving φ in (11) based on α and β is the critical part of the work and consumes most of the computational time. The α and β may vary for different cases, however, the performance improvement of the FDR compared with FEM regarding accuracy and speed-up is independent of α and β provided that the problem is well-posed.

Note that in the bipolar case study, the ion density on the conductor surface is set as the boundary condition. This boundary condition is usually replaced by the Kaptsov's assumption. In

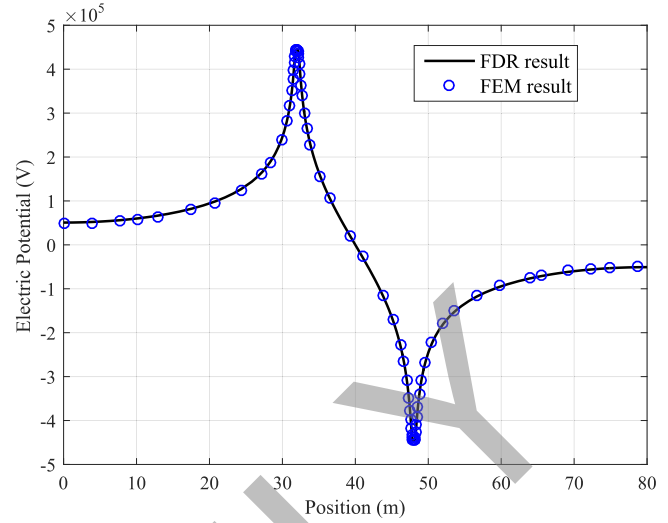


Fig. 11. Result comparison of electric potential along the sample line.

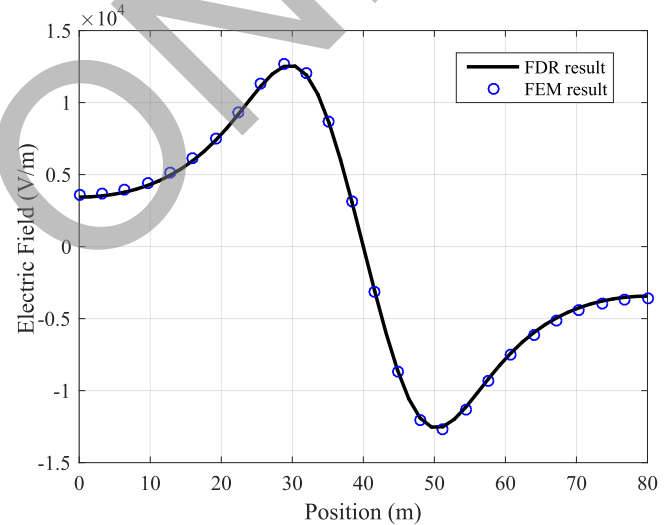


Fig. 12. Result comparison of electric field distribution on the ground.

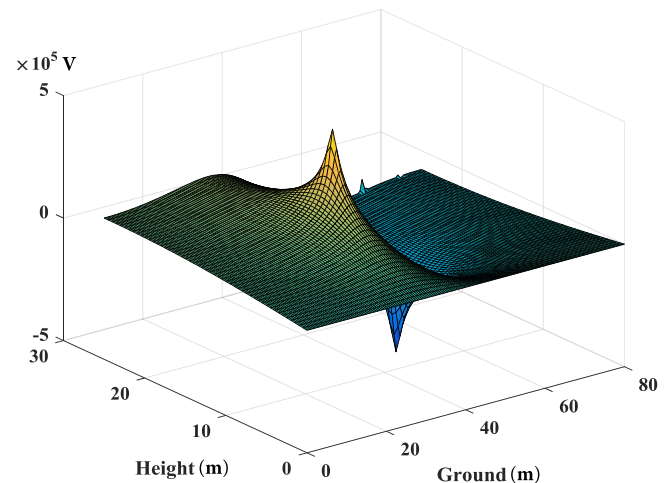


Fig. 13. Electric potential distribution for the bipolar case.

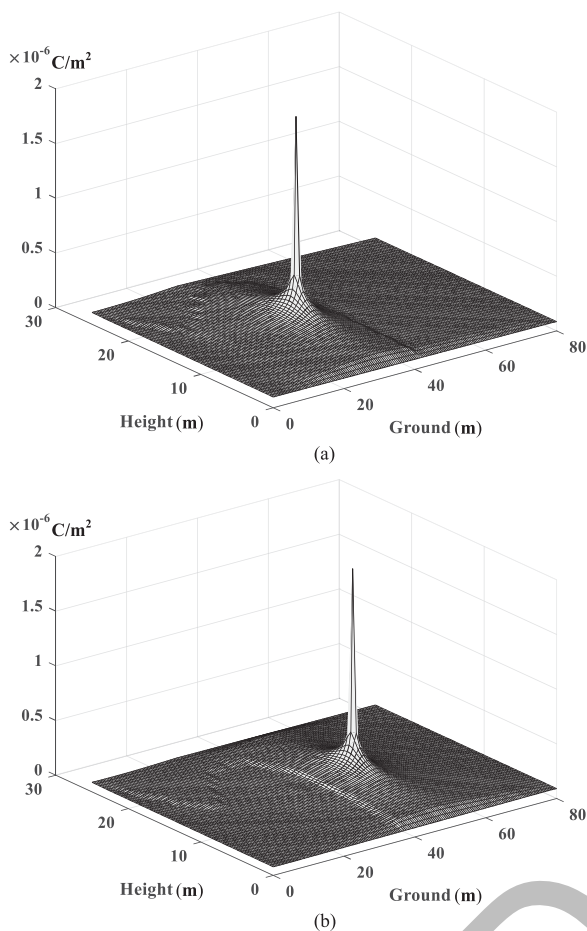


Fig. 14. Ion density distribution for the bipolar case. (a) Positive ion density distribution. (b) Negative ion density distribution.

that case, the ion density on the conductor should be updated in each iteration based on $E_k - E_0$, where E_k is the calculated electric field strength on the conductor surface in the k^{th} iteration and E_0 the corona onset value.

VI. CONCLUSION

In this paper, a finite-difference relaxation (FDR) method is proposed for the computation of both unipolar and bipolar ionized fields in HVDC transmission lines. Instead of solving the current continuity equation as a first order PDE on ion density, this paper solves it as a second order PDE on electric potential. The numerical instability problem is perfectly solved because the FDR scheme applied for (11) is unconditionally stable. The proposed FDR method has the following advantages over the finite element method.

- 1) The scheme is suitable for massively parallel computation: compared with the commercial FEM software Comsol Multiphysics, the speedup is more than 14 times in CPU parallelization and 35 times in GPU parallel implementation. The maximum relative difference compared with the FEM is around 3%, and acceptable for engineering computation.

- 2) The set of equations in the FDR scheme does not have to be assembled. Instead, it is solved by a relaxation scheme and requires much less memory than FEM. For n nodes, the necessary memory required is $\Theta(n)$ for the FDR method and $\Theta(n^2)$ for the FEM.
- 3) Differentiated grid size and interpolation are employed to improve the accuracy and scalability of FDR applied to a vast domain containing a disproportionately thin conductor. Thus FDR can be more flexible when used to handle any domain containing irregular geometries or disproportionate geometry sizes. It is reasonable to conclude that all well-posed second-order PDE having the form of (11) can benefit from the proposed FDR scheme in lieu of FEM with regard to computational efficiency, accuracy, and scalability.

APPENDIX

A. Computation Resources

The GPU version is GeForce GTX Titan Black, with 2880 cores, 889 MHz clock frequency, and 4 GB memory. The CPU version is Intel E5-2620, with 16 cores, 2.1 GHz clock frequency, and 32 GB memory.

B. Unipolar Case Study

The domain width is 2 m, the domain height 2 m, the conductor radius 0.005m, the applied voltage on conductor 20 kV, and the space charge density on conductor $2e-6$ C/m². The initial distribution of space charge density is guessed as $10^{-8} / \sqrt{(x-1)^2 + (y-1)^2}$ C/m². The sample line is defined by two points: (0, 0) and (1, 1).

C. Practical Bipolar Case Study

The applied voltage on conductor is ± 500 kV, the permittivity of free space $8.854e-12$ F/m, the positive ionic mobility $1.4e-4$ m²/V·s, the negative ionic mobility $1.8e-4$ m²/V·s, the recombination rate $2e-12$ m²/s², the charge of electron $1.602e-19$ C, and the space charge density on each conductor $2e-6$ C/m². The sample line is defined by two points: (0, 12.5) and (80, 12.5).

REFERENCES

- [1] P. S. Maruvada and W. Janischewskyj, "Analysis of corona losses on dc transmission lines: I—Unipolar lines," *IEEE Trans. Power App. Syst.*, vol. PAS-88, no. 5, pp. 718–731, May 1969.
- [2] J. S. Townsend, "The potentials required to maintain currents between coaxial cylinders," *Philosophical Mag. Series 6*, vol. 28, no. 163, pp. 83–90, 1914.
- [3] W. Deutsch, "Über die dichtevertelung unipolarer ionenströme," *Annalen der Physik*, vol. 408, no. 5, pp. 588–612, 1933.
- [4] Z. Luo, X. Cui, W. Zhang, and J. Lu, "Calculation of the 3-d ionized field under hvdc transmission lines," *IEEE Trans. Magn.*, vol. 47, no. 5, pp. 1406–1409, May 2011.
- [5] P. S. Maruvada, "Electric field and ion current environment of hvdc transmission lines: Comparison of calculations and measurements," *IEEE Trans. Power Del.*, vol. 27, no. 1, pp. 401–410, Jan. 2012.
- [6] J. Qiao, J. Zou, and B. Li, "Calculation of the ionised field and the corona losses of high-voltage direct current transmission lines using a finite-difference-based flux tracing method," *IET Gener., Transmiss. Distrib.*, vol. 9, no. 4, pp. 348–357, 2015.

- [7] W. Janischewskij and G. Gela, "Finite element solution for electric fields of coronating dc transmission lines," *IEEE Trans. Power App. Syst.*, vol. PAS-98, no. 3, pp. 1000–1012, May 1979.
- [8] T. Takuma, T. Ikeda, and T. Kawamoto, "Calculation of ion flow fields of hvdc transmission lines by the finite element method," *IEEE Power Eng. Rev.*, vol. PER-1, no. 12, pp. 28–28, Dec. 1981.
- [9] T. Takuma and T. Kawamoto, "A very stable calculation method for ion flow field of hvdc transmission line," *IEEE Power Eng. Rev.*, vol. PER-7, no. 1, pp. 51–52, Jan. 1987.
- [10] B. Qin, J. Sheng, Z. Yan, and G. Gela, "Accurate calculation of ion flow field under hvdc bipolar transmission lines," *IEEE Trans. Power Del.*, vol. 3, no. 1, pp. 368–376, Jan. 1988.
- [11] M. Yu and E. Kuffel, "A new algorithm for evaluating HVDC ionized fields in the presence of strong wind," presented at the *5th Biennial IEEE Conf. Electromagn. Field Computation*, Claremont, CA, USA, Aug. 1992.
- [12] Z. Al-Hamouz, "Corona power loss computation in bundled bipolar conductors," in *Proc. Conf. Rec. Ind. Appl. Conf.*, 2000, vol. 2, pp. 719–724.
- [13] Z. Al-Hamouz, "Corona power loss, electric field, and current density profiles in bundled horizontal and vertical bipolar conductors," *IEEE Trans. Ind. Appl.*, vol. 38, no. 5, pp. 1182–1189, Sep. 2002.
- [14] T. Lu, H. Feng, X. Cui, Z. Zhao, and L. Li, "Analysis of the ionized field under hvdc transmission lines in the presence of wind based on upstream finite element method," *IEEE Trans. Magn.*, vol. 46, no. 8, pp. 2939–2942, Aug. 2010.
- [15] G. Huang, J. Ruan, Z. Du, and C. Zhao, "Highly stable upwind fem for solving ionized field of hvdc transmission line," *IEEE Trans. Magn.*, vol. 48, no. 2, pp. 719–722, Feb. 2012.
- [16] J. Liu, J. Zou, J. Tian, and J. Yuan, "Analysis of electric field, ion flow density, and corona loss of same-tower double-circuit hvdc lines using improved fem," *IEEE Trans. Power Del.*, vol. 24, no. 1, pp. 482–483, Jan. 2009.
- [17] Y. Zhen, X. Cui, T. Lu, X. Zhou, and Z. Luo, "High efficiency fem calculation of the ionized field under hvdc transmission lines," *IEEE Trans. Magn.*, vol. 48, no. 2, pp. 743–746, Feb. 2012.
- [18] J. Davis and J. Hoburg, "Hvdc transmission line computations using finite element and characteristics method," *J. Electrostatics*, vol. 18, pp. 1–22, 1986.
- [19] X. Zhou, X. Cui, T. Lu, Y. Zhen, and Z. Luo, "A time-efficient method for the simulation of ion flow field of the ac-dc hybrid transmission lines," *IEEE Trans. Magn.*, vol. 48, no. 2, pp. 731–734, Feb. 2012.
- [20] X. Zhou, T. Lu, X. Cui, Y. Zhen, and G. Liu, "Simulation of ion-flow field using fully coupled upwind finite-element method," *IEEE Trans. Power Del.*, vol. 27, no. 3, pp. 1574–1582, Jul. 2012.
- [21] Z. Du *et al.*, "Calculation of the ionized field around the dc voltage divider," *IEEE Trans. Magn.*, vol. 49, no. 5, pp. 1933–1936, May 2013.
- [22] X. Zhou, T. Lu, X. Cui, Y. Liu, and X. Li, "Simulation of ion-flow field at the crossing of hvdc and hvac transmission lines," *IEEE Trans. Power Del.*, vol. 27, no. 4, pp. 2382–2389, Oct. 2012.
- [23] B. Zhang, W. Li, J. He, and R. Zeng, "2D/3D hybrid computation of ion flow field around house near HVDC bipolar transmission lines," presented at the *14th Biennial IEEE Conf. Electromagn. Field Comput.*, Chicago, IL, USA, May 2010.
- [24] Y. Zhen, X. Cui, T. Lu, Z. Luo, and X. Zhou, "Total electric field calculation of body model under hvdc transmission lines," in *Proc. Asia-Pacific Power Energy Eng. Conf.*, Mar. 2011, pp. 1–4.
- [25] Y. Zhen *et al.*, "Ion flow field analysis considering the finite conductivity of the building near hvdc transmission lines," *IEEE Trans. Magn.*, vol. 51, no. 3, pp. 1–4, Mar. 2015.
- [26] M. F. Kacamarga, B. Pardamean, and J. Baurley, "Comparison of conjugate gradient method and jacobi method algorithm on mapreduce framework," *Appl. Math. Sci.*, vol. 8, no. 17, pp. 837–849, 2014.
- [27] I. Kiss, S. Gyimothy, Z. Badics, and J. Pavo, "Parallel realization of the element-by-element FEM technique by cuda," *IEEE Trans. Magn.*, vol. 48, no. 2, pp. 507–510, Feb. 2012.
- [28] V. Jalili-Marandi and V. Dinavahi, "Simd-based large-scale transient stability simulation on the graphics processing unit," *IEEE Trans. Power Syst.*, vol. 25, no. 3, pp. 1589–1599, Aug. 2010.
- [29] Z. Zhou and V. Dinavahi, "Parallel massive-thread electromagnetic transient simulation on gpu," *IEEE Trans. Power Del.*, vol. 29, no. 3, pp. 1045–1053, Jun. 2014.
- [30] H. Karimipour and V. Dinavahi, "Extended kalman filter-based parallel dynamic state estimation," *IEEE Trans. Smart Grid*, vol. 6, no. 3, pp. 1539–1549, May 2015.
- [31] H. Karimipour and V. Dinavahi, "Parallel relaxation-based joint dynamic state estimation of large-scale power systems," *IET Gener. Transmiss. Distrib.*, vol. 10, no. 2, pp. 452–459, Feb. 2016.
- [32] G. H. Golub and C. F. van Loan, *Matrix Computations*. Baltimore, MD, USA: Johns Hopkins Univ. Press, 1989.
- [33] ATCOElectric, "Structures," 2016. [Online]. Available: <http://www.atcoelectric.com/Projects/HVDC/Project-Details/Structures>



Peng Liu (S'15) received the B.Sc. and M.Eng. degrees in electrical engineering from the Harbin Institute of Technology, Harbin, China, in 2013 and 2015, respectively. He is currently working toward the Ph.D. degree in the Department of Electrical and Computer Engineering, University of Alberta, Edmonton, AB, Canada. His research interests include finite element method, finite-difference method, and parallel and distributed computing.



Venkata Dinavahi (SM'08) received the Ph.D. degree from the University of Toronto, Toronto, ON, Canada, in 2000. He is currently a Professor in the Department of Electrical and Computer Engineering, University of Alberta, Edmonton, AB, Canada. His research interests include real-time simulation of power systems and power electronic systems, large-scale system simulation, and parallel and distributed computing.